AD-A132 076 A GTD ANALYSIS OF THE LAMPS ANTENNA BLOCKED BY A MAST (U) OHIO STATE UNIV COLUMBUS ELECTROSCIENCE LAB R G KOUYOUMJIAN ET AL. 31 MAR 77 ESL-4508-3 1/1

UNCLASSIFIED N00123-76-C-1371 F/G 9/5 NL

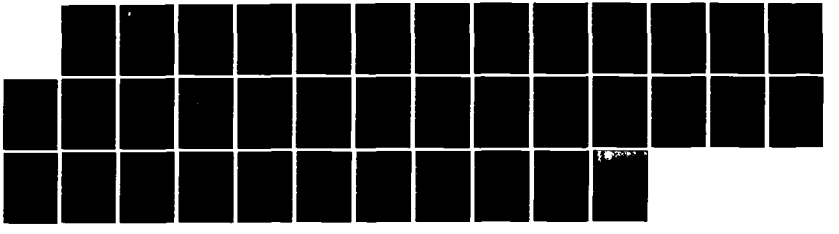

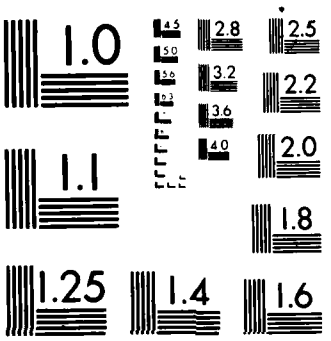

A GTD ANALYSIS OF THE LAMPS ANTENNA BLOCKED BY A MAST

R.G. Kouyoumjian
R.J. Luebbers
R.C. Rudduck

The Ohio State University

ElectroScience Laboratory

Department of Electrical Engineering
Columbus, Ohio 43212

Technical Report 4508-3

31 March 1977

Contract N00123-76-C-1371

Approved for public release;
distribution unlimited.

Naval Regional Procurement Office
Long Beach, California 90822

NOTICES

When Government drawings, specifications, or other data are used for any purpose other than in connection with a definitely related Government procurement operation, the United States Government thereby incurs no responsibility nor any obligation whatsoever, and the fact that the Government may have formulated, furnished, or in any way supplied the said drawings, specifications, or other data, is not to be regarded by implication or otherwise as in any manner licensing the holder or any other person or corporation, or conveying any rights or permission to manufacture, use, or sell any patented invention that may in any way be related thereto.

UNCLASSIFIED

SECURITY CLASSIFICATION OF THIS PAGE (When Data Entered)

REPORT DOCUMENTATION PAGE		READ INSTRUCTIONS BEFORE COMPLETING FORM
1 REPORT NUMBER	2 GOVT ACCESSION NO. AD-A132076	3 RECIPIENT'S CATALOG NUMBER
4 TITLE (and Subtitle) A GTD ANALYSIS OF THE LAMPS ANTENNA BLOCKED BY A MAST		5 TYPE OF REPORT & PERIOD COVERED Technical Report
		6 PERFORMING ORG. REPORT NUMBER ESL 4508-3
7 AUTHOR(s) R.G. Kouyoumjian, R.J. Luebbers R.C. Rudduck		8 CONTRACT OR GRANT NUMBER(s) N00123-76-C-1371
9 PERFORMING ORGANIZATION NAME AND ADDRESS The Ohio State University ElectroScience Laboratory, Department of Electrical Engineering, Columbus, Ohio 43212		10 PROGRAM ELEMENT, PROJECT, TASK AREA & WORK UNIT NUMBERS Project N00953/6/009121
11 CONTROLLING OFFICE NAME AND ADDRESS Naval Regional Procurement Office Long Beach, California 90822		12 REPORT DATE 31 March 1977
		13 NUMBER OF PAGES 32
14 MONITORING AGENCY NAME & ADDRESS (if different from Controlling Office)		15 SECURITY CLASS (of this report) Unclassified
		15a DECLASSIFICATION/DOWNGRADING SCHEDULE

16 DISTRIBUTION STATEMENT (of this Report)

Approved for public release; distribution unlimited.

17 DISTRIBUTION STATEMENT (of the abstract entered in Block 20, if different from Report)

18 SUPPLEMENTARY NOTES

19 KEY WORDS (Continue on reverse side if necessary and identify by block number)

Cylindrical diffraction coefficient
Aperture blockage
LAMPS antenna
GTD
Far-field pattern
Diffraction

20 ABSTRACT (Continue on reverse side if necessary and identify by block number)

A general purpose dyadic diffraction coefficient for plane and spherical waves obliquely incident on a perfectly-conducting circular cylinder is derived. This diffraction coefficient is then employed to calculate the radiation pattern of a LAMPS antenna with a cylindrical mast positioned in front of it.

DD FORM 1 JAN 73 1473 EDITION OF 1 NOV 65 IS OBSOLETE

UNCLASSIFIED

SECURITY CLASSIFICATION OF THIS PAGE (When Data Entered)

CONTENTS

		Page
I.	INTRODUCTION	1
II.	CYLINDER DIFFRACTION COEFFICIENTS	1
	A. Soft Diffraction Coefficient	2
	B. Hard Diffraction Coefficient	7
III.	MODELING AN APERTURE ANTENNA	11
IV.	CYLINDER BLOCKAGE EFFECTS ON THE LAMPS ANTENNA	15
V.	CONCLUSIONS	27
REFERENCES		28
APPENDIX		29

I. INTRODUCTION

The development of a computer code which can be used to calculate the effects of a circular cylinder on the radiation pattern of an aperture antenna is described in this report. The motivation for this research is to investigate the pattern degradation of shipboard antennas caused by nearby masts.

The report is divided into two parts. The first part is concerned with the derivation of expressions for the fields diffracted by a relatively small (in terms of λ) circular cylinder. The resulting solutions for this diffracted field are put into the GTD format so that the cylinder diffraction coefficients can be identified. Thus, the results can be incorporated into a general, ray-optical analysis of a radiating system.

The second part of the report is concerned with using the above results to predict the degradation of the pattern of the LAMPS antenna caused by the presence of a nearby cylinder. The LAMPS antenna is a 34" parabolic dish with a nominal frequency of 4.6 GHz. The resulting computer code is capable of calculating the radiation pattern of the LAMPS antenna both with and without the diffracting cylinder present, so that the effects of the cylinder on the radiation pattern can be easily seen. While the present computer code is limited to calculating patterns in a plane perpendicular to the cylinder axis, with the cylinder being parallel to the plane of the aperture, the theory presented herein is adequate to provide for an extension of the code to the more general case.

II. CYLINDER DIFFRACTION COEFFICIENTS

The goal of this derivation is the development of diffraction coefficients which can be used to find the diffracted fields due to an incident wave interacting with a perfectly-conducting circular cylinder. Two cases will be considered: the soft boundary case (H field perpendicular to the cylinder axis) and the hard boundary case (E field perpendicular to the cylinder axis). The method will be quite straightforward; a canonical problem will be solved and asymptotic approximations will be made so that the resulting solution can be interpreted ray-optically. Then this solution will be compared with a GTD solution to obtain the unknown diffraction coefficients.

It will be seen that the resulting diffraction coefficients are analogous to those encountered in wedge diffraction, which is not surprising since in both cases one is dealing with a line of scattering (the axis of the wire or the edge of the wedge).

B. Soft Diffraction Coefficient

The geometry of the canonical problem we wish to consider is shown in Figure 1. The field incident on a perfectly-conducting cylinder of radius

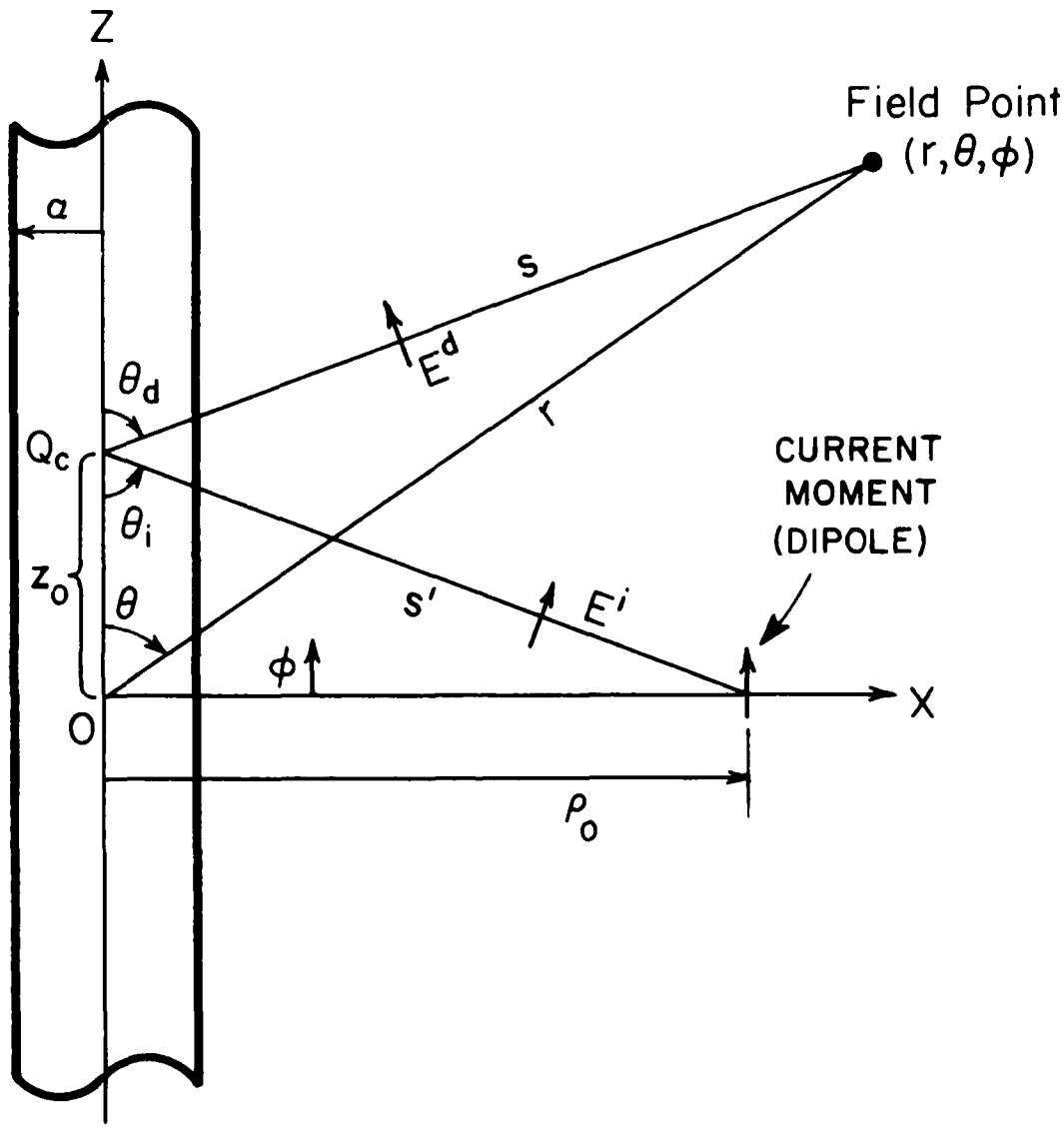

Figure 1. z directed current moment (dipole in the presence of a circular cylinder centered on the z axis.

a is due to a z-directed electric current moment $p_e=I\ell$ at $\rho=\rho_o$, $\phi=0$, $z=0$. The current I extends over the incremental distance $\ell<<\lambda$. The cylindrical diffraction point Q_c is located on the axis of the cylinder at the point where $\theta_d=\theta_i$. The cylinder (or wire) like the edge of a wedge is a line of

scattering, so the angle of diffraction θ_d equals the angle of incidence θ_i. The field point is located using the ordinary spherical coordinates (r,θ,ϕ).

Considering the problem ray-optically [2], we can express the-component of the diffracted electric field E^d as

$$E^d(s) = E^i(Q_c)D_s\sqrt{\frac{s'}{s(s'+s)}}\ e^{-jks} \tag{1}$$

in which $E^i(Q_c)$ is the incident electric field at Q_c, D_s is the soft diffraction coefficient, and s' is the caustic distance. see Equation 6.42 of [2]. Note that $\bar{E}^i$ is in the plane of incidence formed by the cylinder axis and the ray incident from the current moment (or dipole) to Q_c. The above expression is analogous to that used to calculate the fields diffracted by a wedge; the diffraction coefficient remains to be found.

When Q_c is in the far-zone of the current moment, the incident field

$$E^i(Q_c) = -j\frac{kp_e\eta}{4\pi}\ \frac{e^{-jks'}}{s'}\sin\theta_i\ ; \tag{2}$$

in which $k = 2\pi/\lambda$ is the wave number and η is the characteristic impedance of free space. Combining (1) with (2)

$$E^d(s) = -j\frac{kp_e\eta}{4\pi}\sin\theta_i D_s\frac{1}{\sqrt{ss'(s+s')}}\ e^{-jk(s'+s)} \tag{3}$$

One can obtain an eigenfunction solution for this same geometry. When the field point is in the far zone, the θ component of the total electric field is given by

$$E_\theta = j\frac{kp_e\eta\sin\theta}{4\pi}\ \frac{e^{-jkr}}{r}\left[e^{jk\rho_o\sin\theta\cos\phi} - S_e\right] \tag{4}$$

where

$$S_e = \sum_{m=0}^{\infty}\varepsilon_m j^m\ \frac{J_m(ka\sin\theta)}{H_m^{(2)}(ka\sin\theta)}\ H_m^{(2)}(k\rho_o\sin\theta)\cos m\phi, \tag{5}$$

the phase reference is the origin, and

$$\varepsilon_m = \begin{cases} 1, & m=0 \\ 2, & m\neq 0. \end{cases}$$

In the far-zone note that $\theta=\theta_i=\theta_d$.

The result given in (4) and (5), which is derived in the Appendix, has been obtained previously by reciprocity arguments [3], the Hertz vector [4] and the Green's function method [5].

In (4) it is apparent that the first term is the incident field of the dipole, so the second term must be the field diffracted from the cylinder. Referring the phase of the second term to Q_C with

$$r \simeq s + z_o \cos\theta \ , \tag{7}$$

$$E_\theta^d(s) = -j \frac{kp_e\eta}{4\pi} \sin\theta \ S_e \ e^{-jkz_o\cos\theta} \frac{e^{-jks}}{s} \tag{8}$$

The above equation may be compared now with the far-zone form of (3)*

$$E^d(s) = -j \frac{kp_e\eta}{4\pi} \sin\theta \ D_s \frac{e^{-jks'}}{\sqrt{s'}} \frac{e^{-jks}}{s} \tag{9}$$

to obtain

$$D_s = -\sqrt{s'} \ e^{jks'} \ S_e \ e^{-jkz_o\cos\theta} \ . \tag{10}$$

In this form D_s is dependent on the distance s' from Q_C to the source, the distance z_o from Q_C to the origin, and the distance ρ_o from the origin to the source; where ρ_o appears in the expression for S_e. We will next simplify the above equation for D_s to remove the dependence on these distances, so that D_s will depend only on the cylinder radius a, λ, and the aspects of incidence and diffraction as viewed from Q_C.

A case commonly encountered in practice occurs when $\rho_o >> a$, i.e., the dipole is many radii removed from the cylinder. For this situation we can introduce the large argument asymptotic approximation of the Hankel function,

$$H_m^{(2)}(k\rho_o\sin\theta) \sim \sqrt{\frac{2j}{\pi k\rho_o\sin\theta}} \ j^m \ e^{-jk\rho_o\sin\theta} \ , \tag{11}$$

into the equation for S_e. In the above approximation the argument must be much larger than the order; however this condition is met for the terms in the series which contribute significantly to S_e. Thus S_e reduces to

*Note that the E-field unit vectors defined in Figure 1 are in the $-\theta$ direction.

$$S_e = \sqrt{\frac{2j}{\pi k \rho_0 \sin\theta}}\; e^{-jk\rho_0 \sin\theta} \sum_{m=0}^{\infty} \varepsilon_m (-1)^m \frac{J_m(ka\,\sin\theta)}{H_m^{(2)}(ka\,\sin\theta)} \cos m\phi \qquad (12)$$

Employing the above equation in (10) and utilizing the relationships

$$s' = \rho_0/\sin\theta = \rho_0 \sin\theta + z_0 \cos\theta, \qquad (13)$$

it is found that

$$D_s = -\sqrt{\frac{2j}{\pi k}}\; \frac{1}{\sin\theta_d} \sum_{m=0}^{\infty} \varepsilon_m (-1)^m \frac{J_m(ka\,\sin\theta_d)}{H_m^{(2)}(ka\,\sin\theta_d)} \cos m\phi \qquad (14)$$

when $\rho_0 \gg a$. This is the desired form for the soft diffraction coefficient, since it depends only on a/λ and the aspects of incidence and diffraction. It may be used in (1) even though the field point is not in the far zone, where $s \gg s'$; it is sufficient that $ks \sin\theta_d \gg 1$. This explains why θ_d has been used in place of θ in (14). For a very thin wire where $ka \ll 1$, the formula for D_s simplifies further to

$$D_s = \frac{-e^{-j\frac{\pi}{4}}}{\sqrt{2\pi k}\,\sin\theta_d}\; \frac{\pi}{\ell n\, 2 - \ell n(\nu\, ka\, \sin\theta_d) - j\frac{\pi}{2}} \qquad (15)$$

in which $\nu = 1.781$. It is seen that D_s is independent of ϕ for a sufficiently thin cylinder (wire).

It is evident that D_s given by (14) is much more convenient to use than the form given earlier in (10). However in cases where ρ_0 is not much greater than a, it is desirable to seek a correction to (14) which introduces ρ_0 in a relatively simple way.

Let us consider the Debye or tangent approximation to the Hankel function. This is a more accurate asymptotic approximation and is not limited to the case where $k\rho_0 \sin\theta \gg n$. The Debye asymptotic approximation is

$$H_n^{(2)}(x) \sim \sqrt{\frac{2j}{\pi x \sin\alpha}}\; e^{-jx(\sin\alpha - \alpha\cos\alpha)} \qquad (16)$$

where $x \cos\alpha = n$.

The following approximations are valid for $m/x < 1$ (but x not close to m).

$$\sqrt{\frac{2}{\pi x \sin\alpha}} \approx \sqrt{\frac{2}{\pi x}} \left[1 + \frac{1}{2}\left(\frac{m}{x}\right)\right]^2 \tag{17a}$$

$$x \sin\alpha \approx x - m\left[\left(\frac{m}{2x}\right) + \left(\frac{m}{2x}\right)^3\right] \tag{17b}$$

$$x\,\alpha\cos\alpha \approx m\frac{\pi}{2} - m\,2\left[\left(\frac{m}{2x}\right) + \frac{4}{3}\left(\frac{m}{2x}\right)\right]^2 . \tag{17c}$$

Substituting the above into (16) and noting that

$$e^{jm\frac{\pi}{2}} = j^m,$$

$$H_m^{(2)}(x) \sim \sqrt{\frac{2j}{\pi x}}\; j^m\, e^{-jx}\left[1 + \frac{1}{2}\left(\frac{m}{x}\right)^2\right]\; e^{-jm\left[\left(\frac{m}{2x}\right) + \frac{1}{3}\left(\frac{m}{2x}\right)^3\right]} \tag{18}$$

It is evident that the term in the bracket and the following exponential term are approximately equal to unity for $x \gg m$; hence the term preceding the bracket is the large argument approximation (see (11) where $x = k\rho_0 \sin\theta$). Since the series representation of S_e given in (5) converges for $m \approx 2ka\sin\theta$, it follows from the condition $x > m$ that $\rho_0 > 2a$, since $x = k\rho_0 \sin\theta$ here. The condition $\rho_0 > 2a$ is usually met in practice.

The relative size of the correction terms in (18) which contain the ratio m/x (with $m \approx 2$ ka $\sin\theta$ and $x = k\rho_0 \sin\theta$) indicates whether the form of D_s with the large argument approximation for the Hankel function is valid. If the correction terms are too large to be neglected and $\rho_0 > 2a$, the Debye form of the Hankel function in (18) can be used in (10) with the result that

$$D_s = -\sqrt{\frac{2j}{\pi k}}\;\frac{1}{\sin\theta_d}\;\sum_{m=0}^{\infty}\epsilon_m(-1)^m\;\frac{J_m(ka\sin\theta_d)}{H_m^{(2)}(ka\sin\theta_d)}\;\cos m\phi\; x$$

$$x\left[1 + \frac{1}{2}\left(\frac{m}{k\rho_0\sin\theta_d}\right)^2\right]\exp\left\{-jm\left[\left(\frac{m}{2k\rho_0\sin\theta}\right) + \frac{1}{3}\left(\frac{m}{2k\rho_0\sin\theta_d}\right)^3\right]\right\} \tag{19}$$

B. Hard Diffraction Coefficient

One can proceed in a similar manner to find the hard diffraction coefficient D_h by replacing the z-directed, electric current moment by a z-directed magnetic current moment. Note that E^i is now perpendicular to the aforementioned plane of incidence. For this case the z-component of the diffracted field is given by

$$E^d(s) = E^i(Q_c)D_h\sqrt{\frac{s'}{s(s+s')}}\ e^{-jks} \tag{20}$$

in which $E^i(Q_c)$ is the (scalar) incident electric field at the point of diffraction Q_c. Following the same steps used to obtain (10) for the soft diffraction coefficient, we find that

$$D_h = \sqrt{s'}\ e^{-jks'}\ S_m\ e^{-jkz_o\cos\theta}\ , \tag{21}$$

where the expression for S_m derived in the Appendix is

$$S_m = -\sum_{m=0}^{\infty}\ \varepsilon_m j^m \frac{J_m'(ka\sin\theta)}{H_m^{(2)'}(ka\sin\theta)}\ H_m^{(2)}(k\rho_o\sin\theta)\cos m\phi \tag{22}$$

in which the prime denotes differentiation with respect to the argument.

For the case where $\rho_o >> a$, the large argument approximation for $H_m^{(2)}(k\rho_o\sin\theta)$ may be used as before to obtain

$$D_h = -\sqrt{\frac{2j}{\pi k}}\ \frac{1}{\sin\theta_d}\ \sum_{m=0}^{\infty}\ \varepsilon_m(-1)^m \frac{J_m'(ka\sin\theta_d)}{H_m^{(2)'}(ka\sin\theta_d)}\ \cos m\phi \tag{23}$$

which compares with (14) for the other polarization (soft case). For a very thin wire where $ka << 1$, the above expression simplifies further to

$$D_h = \frac{-e^{-j\frac{\pi}{4}}}{\sqrt{2\pi k}\sin\theta_d}\ \frac{\pi(ka\sin\theta_d)^2}{2}\ (1+2\cos\phi) \tag{24}$$

Comparing the above equation with (15), it is clear that $|D_h| << |D_s|$, as one would expect for the thin wire case. Furthermore one notes that there is null in the diffraction pattern at $\phi = 120°$.

If ρ_o is not $\gg a$ but $\rho_o \geq 2a$, we may employ the Debye approximation of $H_m^{(2)}(k\rho_o \sin\theta)$ with the result that

$$D_h = -\sqrt{\frac{2j}{\pi k}} \frac{1}{\sin\theta_d} \sum_{m=0}^{\infty} \varepsilon_m (-1)^m \frac{J_m'(ka \sin\theta_d)}{H_m^{(2)\prime}(ka \sin\theta_d)} \cos m\phi \times$$

$$\times \left[1 + \frac{1}{2}\left(\frac{m}{k\rho_o \sin\theta_d}\right)^2\right] \exp\left\{-jm\left[\left(\frac{m}{2k\rho_o \sin\theta_d}\right) + \frac{1}{3}\left(\frac{m}{2k\rho_o \sin\theta_d}\right)^3\right]\right\} \quad (25)$$

which compares with (19) for the other polarization.

The scalar diffraction coefficients may be employed in a dyadic diffraction coefficient of the same form as that derived for edge diffraction [1]. As mentioned earlier, the plane of incidence is defined to be the plane containing the incident ray to the diffraction point Q_c and the axis of the cylinder, and in addition we may introduce a plane of diffraction defined to be the plane containing the diffracted ray and the axis of the cylinder. The angle between these two planes is ϕ. Let us now decompose the incident electric field into $E^i(Q_c)_{\parallel}$ and $E^i(Q_c)_{\perp}$, components parallel and perpendicular to the plane of incidence; similarly let us separate the diffracted electric field into $E^d(s)_{\parallel}$ and $E^d(s)_{\perp}$, components parallel and perpendicular to the plane of diffraction. Then in matrix form

$$\begin{bmatrix} E_{\parallel}^d \\ E_{\perp}^d \end{bmatrix} = \begin{bmatrix} D_s & 0 \\ 0 & D_h \end{bmatrix} \begin{bmatrix} E_{\parallel}^i \\ E_{\perp}^i \end{bmatrix} \sqrt{\frac{s'}{s(s+s')}}\, e^{-jks} \quad , \quad (26)$$

where the directions of the parallel field components are shown in Figure 1, and the direction of the perpendicular component in each case is determined by taking the vector product of the parallel unit vector (see Figure 1) with a unit vector in the direction of propagation. We conclude this section by presenting some numerical results for the magnitude of D_s and D_h as a function of ϕ for various cylinder radii from $ka = .25$ ($a = .04\lambda$) to $ka = 4$ ($a = .64\lambda$); $\theta_d = 90°$ in each case. Equations (14) and (23) were used to calculate the curves shown in Figures 2 and 3. The number of terms included in the series varied with cylinder size. For the two smaller cylinders 4 terms were used, for the $ka = 1$ cylinder 5 terms, and for the $ka = 4$ cylinder 8 terms. In line with the earlier discussion, larger diameters could be accommodated at the cost of including more terms (approximately $2ka \sin\theta_d$) in the series. It is seen that the curves for $ka = .25$ approximate the behavior predicted by (15) and (24), which was described earlier.

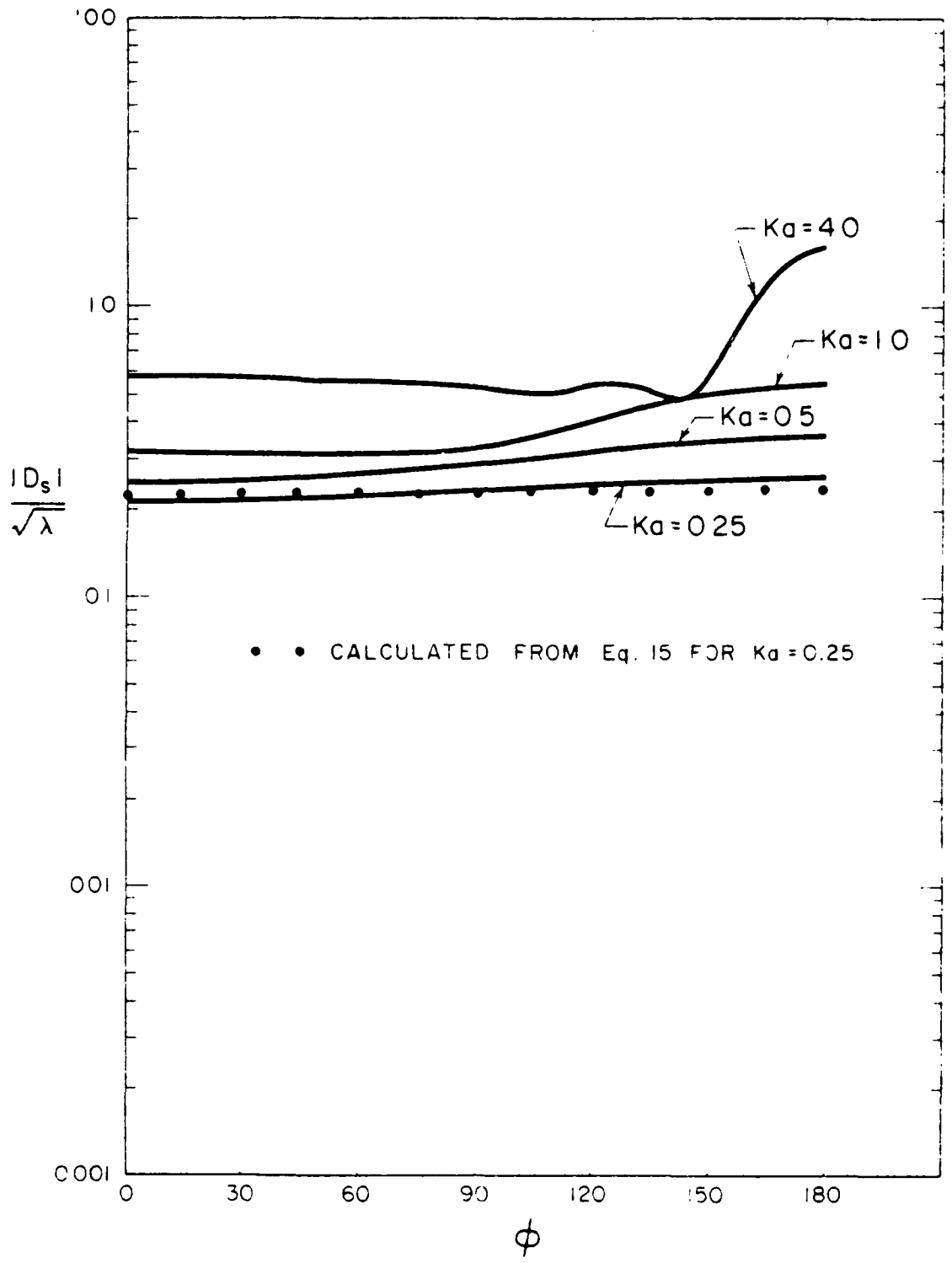

Figure 2. D_S for a circular cylinder of radius a; $\theta_d=90^\circ$; $\rho_0 >> a$.

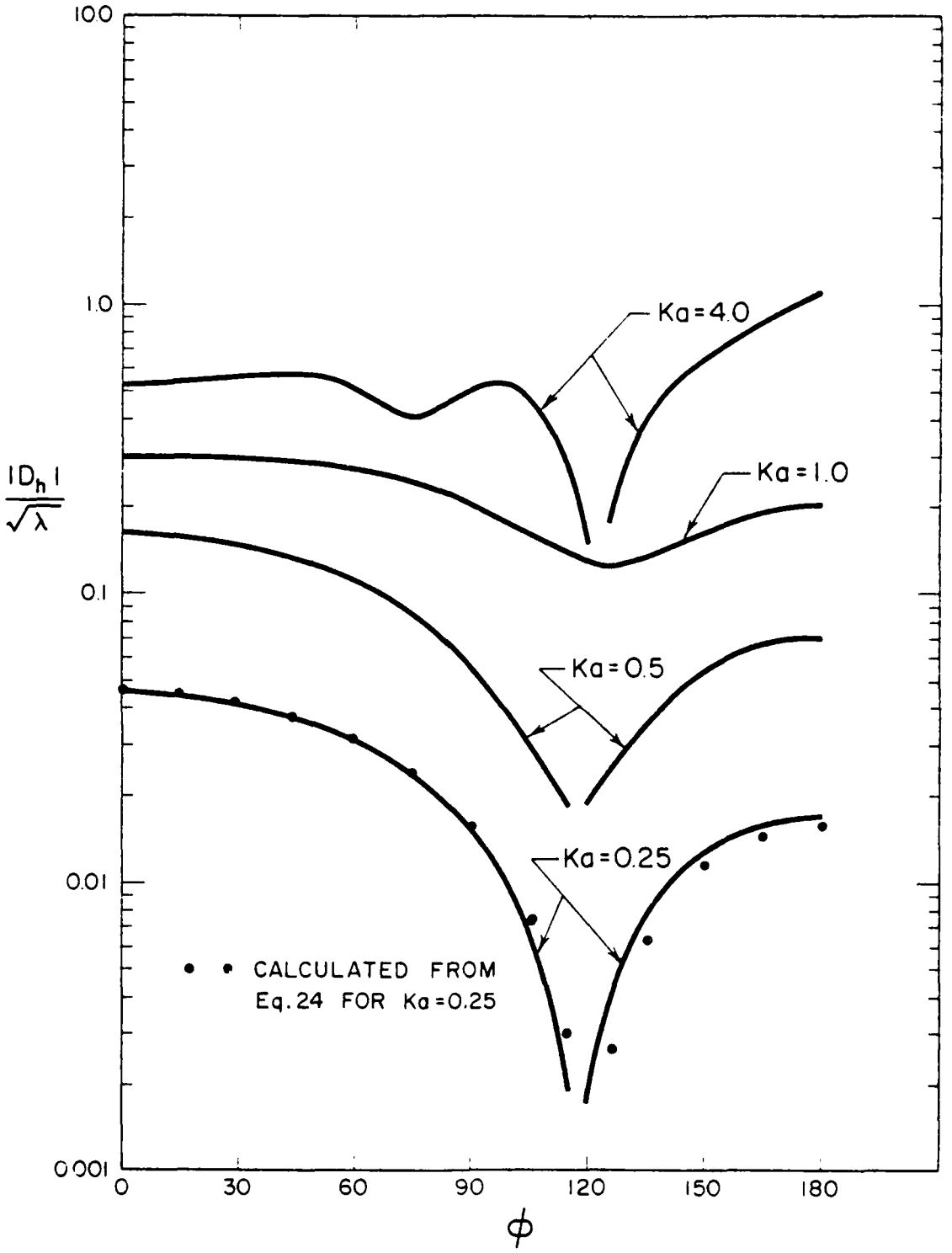

Figure 3. D_h for a circular cylinder of radius a; $\theta_d=90°$; $\rho_o >> a$.

III. MODELING AN APERTURE ANTENNA

Let us now proceed to the computer code developed to calculate the cylindrical aperture blockage. The problem which can be handled with the present program is shown in Figures 4 and 6. The equivalent currents in the aperture are modeled with z-directed electric and magnetic dipoles situated in the YZ-plane. The magnitudes of the various dipoles can be adjusted so as to model tapered or other non-uniform aperture distributions. The cylindrical scatterer of radius a is located at $\rho = \rho_0$, $\phi = \phi_0$, and is parallel to the z axis. The program is capable of computing the far-field patterns in the XY (i.e., $\theta = 90°$) plane, both with and without the cylinder present. Thus only a one-dimensional model of the aperture is required.

The dipole moments Idl and Kdl for the equivalent electric and magnetic dipoles are obtained from the electric field aperture distribution as shown in Figure 5. The aperture is divided into thin vertical strips of width W, where the W is chosen small enough so that the relative phase of the aperture fields are essentially constant across the strip for all pattern aspects. From the uniqueness theorems we know that only the y- and z- (tangential) components of the E field (or H field) need to be specified in the aperture. For a planar aperture, assuming that the fields in the aperture plane outside the aperture region are negligibly small, we have, from the equivalence principle,

$$J_z(y,z) = -2\, E_z(y,z)/n \tag{27}$$

$$K_z(y,z) = -2\, E_y(y,z) \tag{28}$$

where $\bar{J}$ and $\bar{K}$ are the equivalent electric and magnetic surface currents in the aperture, the subscripts denote the y and z components, and n is the free space characteristic impedance.

We can easily obtain the electric and magnetic dipole moments corresponding to the equivalent currents for any aperture strip. For the dipoles located at $y=y_n$ we have

$$Idl = \int_{-z_b}^{z_b} \int_{y_n-w/2}^{y_n+w/2} J_z(y,z) e^{jkz\cos\theta}\, dy\, dz \tag{29}$$

$$Kdl = \int_{-z_b}^{z_b} \int_{y_n-w/2}^{y_n+w/2} K_z(y,z) e^{jkz\cos\theta}\, dy\, dz \tag{30}$$

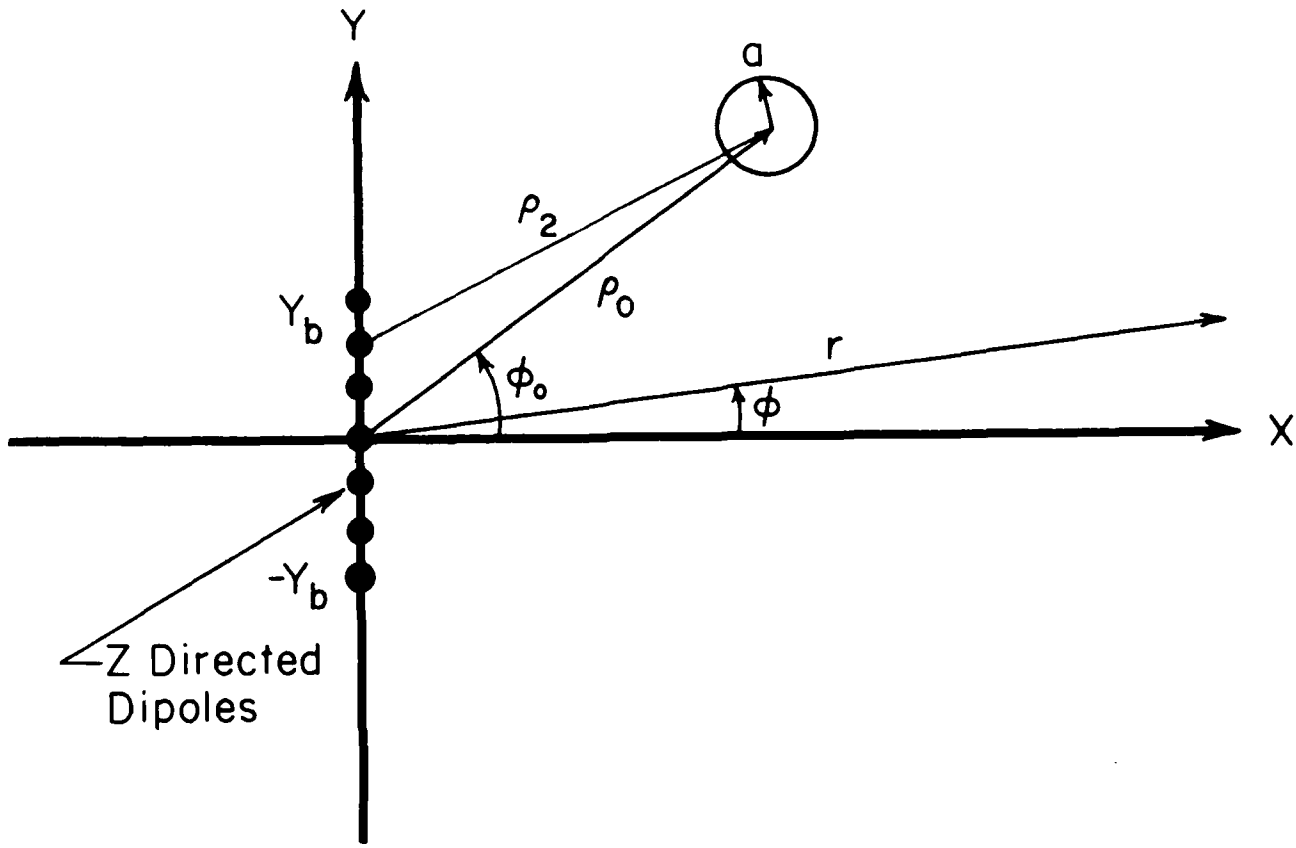

Figure 4. The present computer program is capable of calculating the far field pattern as a function of $\phi(\theta=90°)$ for the geometry shown. The aperture antenna is modeled by the z directed magnetic and electric dipoles located along the y axis. The dipole magnitudes need not be identical, so that tapered aperture distributions may be modeled.

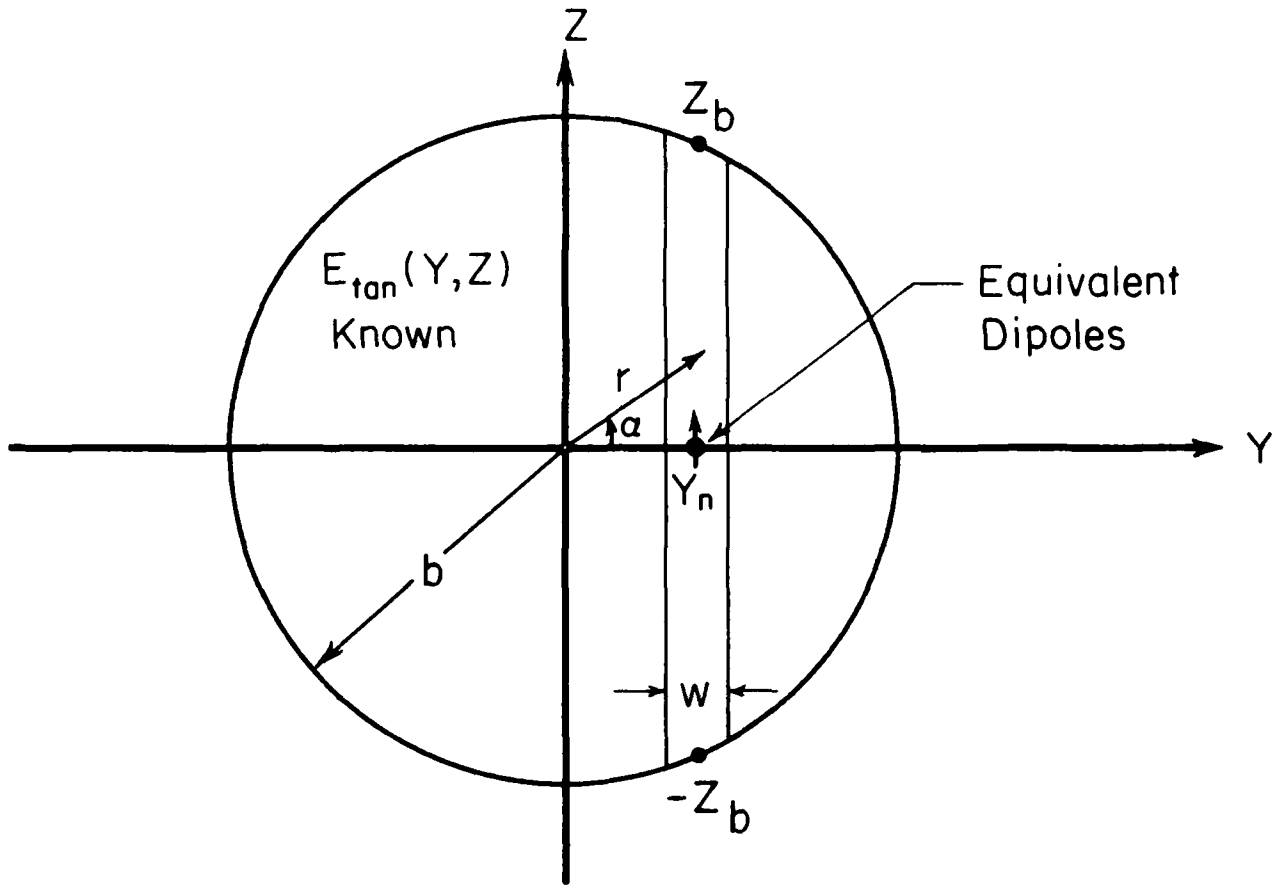

Figure 5. Aperture strip and equivalent magnetic and electric dipoles.

The far-fields of these z-directed dipoles are given by

$$E_\theta = j \frac{k\eta\, Idl}{4\pi} \frac{e^{-jkr}}{r} \sin\theta \tag{31}$$

$$E_\phi = -j \frac{k\ Kdl}{4\pi} \frac{e^{-jkr}}{r} \sin\theta \tag{32}$$

With these equations and the diffraction coefficient developed in the previous section the computer code for the radiation from the sources shown in Figure 4 has been developed in a straightforward manner. The total field E^t due to the electric dipole at y_n is the sum of the direct (or incident) field from the dipole given by (31) with $r = r_n$, $\theta = 90°$ and the field diffracted from the cylinder

$$E_\theta^d = \frac{jk\eta}{4\pi} Idl \frac{e^{-jk\rho_n}}{\sqrt{\rho_n}} D_s(\phi-\phi_n) e^{jk\rho_n\cos(\phi-\phi_n)} \frac{e^{-jkr_n}}{r_n} \tag{33}$$

in which ρ_n is the distance between the dipole at y_n and the axis of the cylinder, ϕ_n is the angle ρ_n makes with the x-axis, r_n is the distance between the dipole at y_n and the field point, and $D_s(\phi-\phi_n)$ is calculated for $\theta = \theta_d = 90°$. Combining (31) and (33)

$$E_\theta^t = j \frac{k\eta\, Idl}{4\pi} \frac{e^{-jkr_n}}{r_n} \left[1 + \frac{e^{-jk\rho_n}}{\sqrt{\rho_n}} D_s(\phi-\phi_n) e^{jk\rho_n\cos(\phi-\phi_n)}\right] \tag{34}$$

The total far-field due to all the z-directed electric current dipoles in the aperture is calculated by summing (34) on n to obtain the contributions from the 2b/w dipoles involved.

IV. CYLINDER BLOCKAGE EFFECTS ON THE LAMPS ANTENNA

Let us now proceed to use the previously presented method to predict the effects of mast blockage on the LAMPS antenna. The problem geometry is shown in Figure 6. The LAMPS antenna itself is an offset fed parabolic reflector antenna with the following estimated parameters:

Diameter: 34 inches
Gain: 28 dB @ 4.6 GHz (Midband)
Polarization: Linear Vertical
Beamwidth: 5° x 5°.

In order to simplify our model of the LAMPS antenna we will assume that the effects of aperture blockage due the feed and its supports can be neglected. This assumption will have little effect on our calculations when cylinder blockage is a significant factor, since the pattern degradation caused by the cylinder will be much greater than that caused by aperture blockage. However, patterns calculated with the blocking cylinder absent will have far out sidelobes at an unrealistically low level [7]. This should be kept in mind when evaluating the effects of the cylinder blockage on the pattern.

For lack of more detailed information we will also assume that the aperture distribution is radially symmetric, and of the type

$$\left[1 - \left(\frac{r}{b}\right)^2\right]^p,$$

where b is the aperture radius and here r is measured radially in the plane of the aperture from its center (see Figure 5). This assumption yields, for the LAMPS aperture, at 4.6 GHz, the following Table [6]:

P	Gain	1/2 Power Beamwidth
0	32.33	4.42°
1	31.08	5.5°
2	29.81	6.37°
3	28.76	7.15°

Since the gain of the antenna is more easily affected by spillover, blockage, losses, etc., than the pattern shape, we will choose p = 1, because this distribution produces the beamwidth which is closest to the given value of 5°.

We can now proceed to use (29) and (30) to evaluate the relative dipole magnitudes Idl and Kdl. Since the antenna is vertically polarized, Kdl $\approx$ 0. Referring to the geometry of Figure 5, we have from Equation (29),

$$Idl = C \int_{-z_b}^{z_b} \int_{y_n-w/2}^{y_n+w/2} \left(1 - \frac{y^2+z^2}{b^2}\right) e^{jkz\cos\theta}\, dy\, dz \qquad (35)$$

since $r^2=y^2+z^2$. The factor C is an unknown constant which need not concern us since we are interested in relative pattern levels rather than absolute field strengths. Since the cylinder and the aperture dipoles are vertical, $\theta = 90°$. If we make the approximation that $r^2 \approx y_n^2 + z^2$ (since $w \ll b$), and note that $z_b = b^2 - y_n^2$, we obtain

$$Idl = C \cdot 2w\sqrt{b^2-y_n^2} - \frac{2wC}{3b^2}\left[(b^2-y_n^2)^{3/2}+3y_n^2(b^2-y_n^2)^{1/2}\right] \qquad (36)$$

for the dipole strength as a function of strip width w and dipole position y_n. Note that the first term in (35) is the dipole strength for a uniform distribution; the second term is due to the assumed

$$1 - \left(\frac{r}{b}\right)^2$$

taper. The result obtained in (36) was used in the previously described computer program. Convergence tests were made, and it was found that 40 strips gave accurate results for the 13.23λ diameter LAMPS antenna. As will be seen the half power beamwidth, the 1st side-lobe level of -24.6 dB, and the 1st null position of 7.1° of the unblocked antenna pattern are quite accurately reproduced [6].

The calculated radiation patterns in Figures 7 through 14 will be discussed next. In Figures 7 and 8 the variation of the blockage effects with the mast-to-LAMPS antenna separation is shown. The separation ρ_o is varied within the given range of 2 ft. to 10 ft. Note that despite the 5 to 1 variation in separation the on-axis blockage varies less than 0.4 dB. This occurs because we are within the near field of the antenna throughout this range of ρ_o variation. Indeed, using the D^2/λ far field criteria, the near field for the LAMPS antenna extends to 37.5 feet. Thus for the range of ρ_o values indicated in the Figures 7 and 8 the antenna beam has not started to spread and the 1/r spherical wave field behavior is not yet evident. Thus any attempt to reduce the on axis blockage by increasing the antenna-cylinder spacing ρ_o will have little effect for spacings of less than 30-40 feet. The blockage effect for on-axis separations of D^2/λ = 37.5 feet and $2D^2/\lambda$ = 75 feet are shown in Figure 9. The scattered field from the cylinder is known to decrease by 3 dB when the separation between the antenna and cylinder is doubled in the far-zone of the antenna. This decrease is apparent in the region $\phi>40°$, where the field directly radiated from the antenna is insignificant. The small irregularities in the two patterns are caused by the large separation of the cylinder and aperture with a resulting rapid phase variation with aspect ϕ of the second term within the brackets of (34).

In Figures 10 and 11 the variation of blockage effects with cylinder radius is shown. The larger cylinders have greater on-axis blockage due to their greater shadowing effect. The exact on-axis blockage loss for the curves of Figures 10 and 11 are as indicated in the figure titles.

In Figures 12, 13 and 14 the effects of varying the angular position of the blocking cylinder are illustrated. In Figure 12 patterns are calculated for ϕ_0 values of 0°, 10°, and 30°. For ϕ_0 = 10° the cylinder is near the edge of the near field "beam" and the blockage is greatly decreased from the ϕ_0 = 0°. For ϕ_0 = 30° the cylinder is well out of the active near field region, and the scattering effects of the cylinder are negligible except for the far-out sidelobe levels.

Figures 13 and 14 confirm that a knowledge of the far field pattern of the LAMPS antenna does not provide insight into near field blockage effects. For example, the far field pattern has a null at ϕ = 7° and a first sidelobe at ϕ = 9°. Thus, were the cylinder in the far field of the antenna, locating the cylinder at ϕ_0 = 7° should produce less effect than with the cylinder at ϕ_0 = 9°. The results shown in Figures 13 and 14 indicate that the opposite results, and that the far field distribution has not yet been formed for a separation of only 6 feet.

At this point, as a reminder, we repeat that the unperturbed patterns shown in Figures 7 through 14 were calculated without including blockage effects of the feed system; thus the sidelobe levels are unrealistically low. For a more valid comparison one should compare the calculated sidelobe levels of the perturbed (by the cylinder) patterns with measured patterns of the LAMPS antenna. However, the figures contained herein do provide a good estimate of the effects of the cylinder, since for the range of ρ_0, ϕ_0, and a values considered the blockage effects of the cylinder are usually much more significant than those of the feed system.

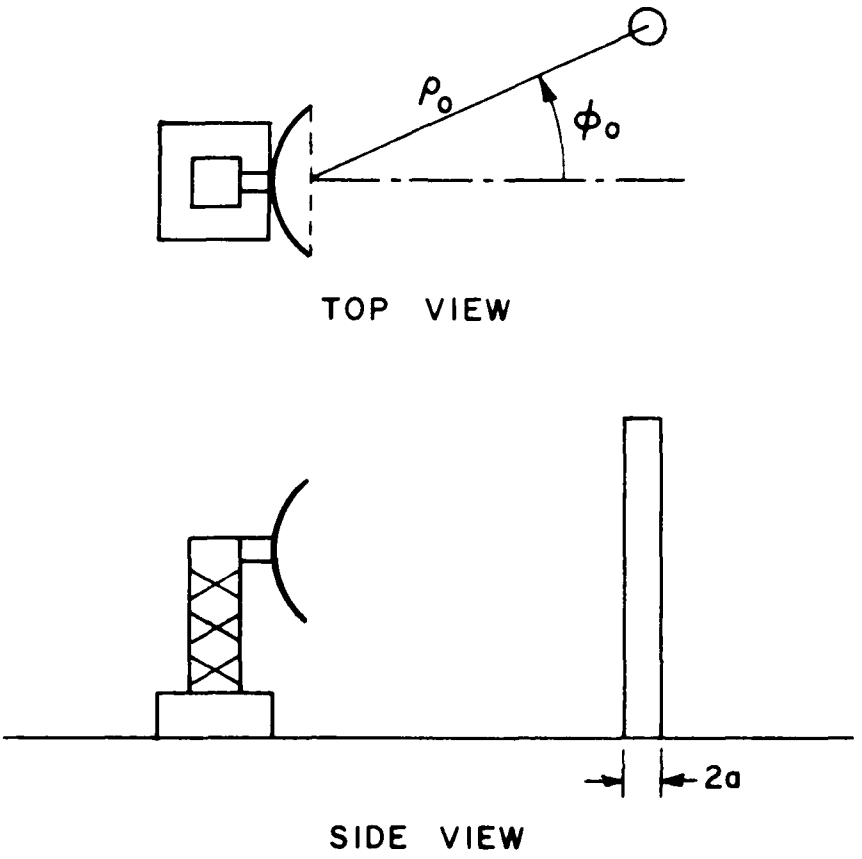

Figure 6. LAMPS antenna with a blocking cylinder.

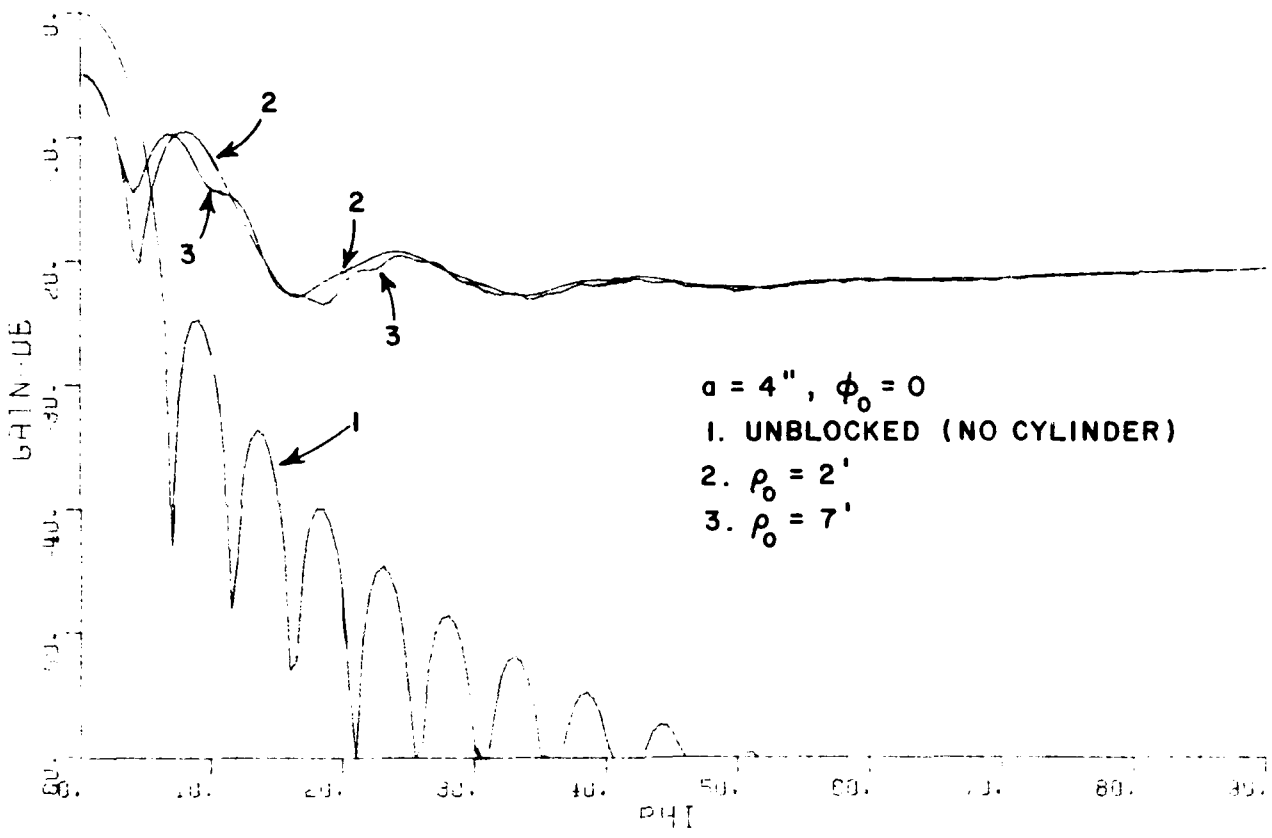

Figure 7. Azimuth pattern of the LAMPS antenna with a blocking cylinder.

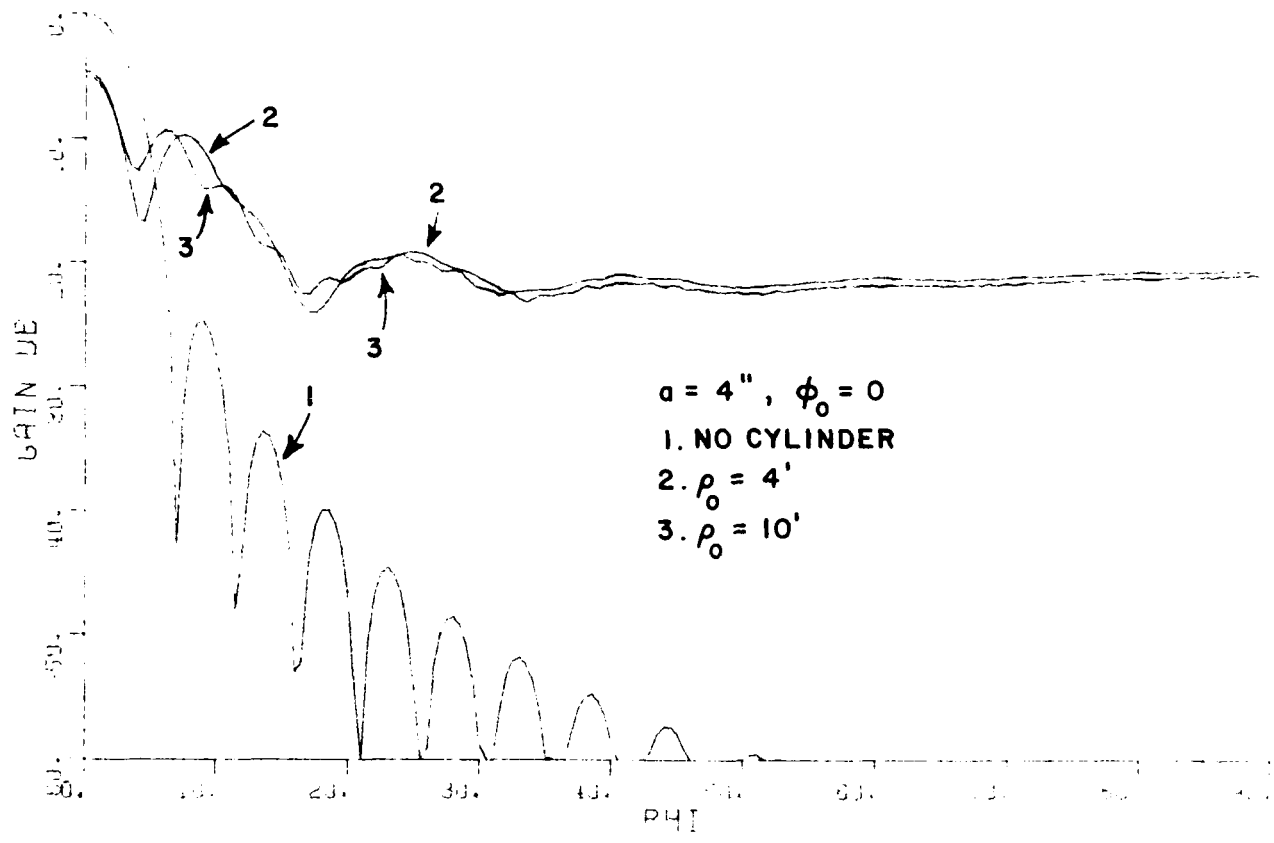

Figure 8. Azimuth pattern of the LAMPS antenna with a blocking cylinder.

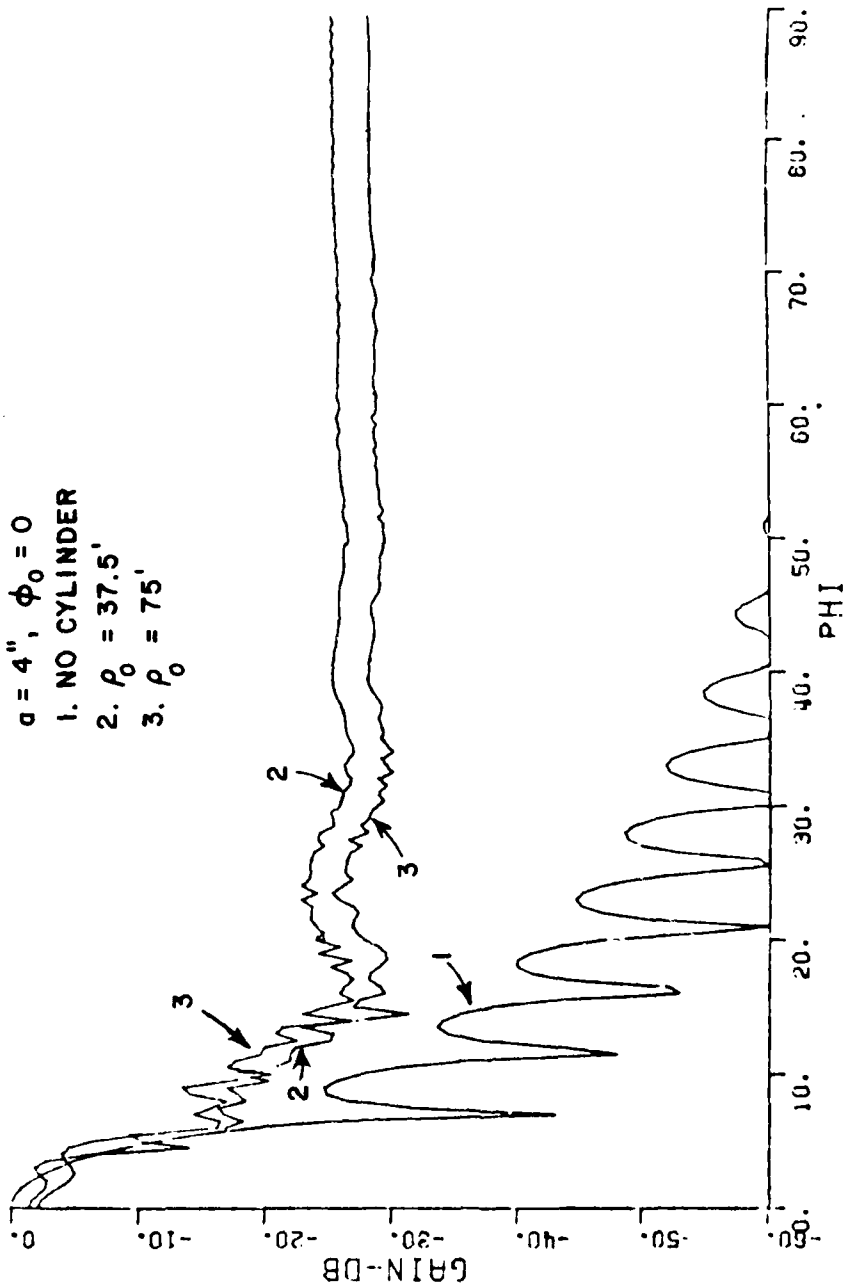

Figure 9. Azimuth pattern of the LAMPS antenna with a blocking cylinder.

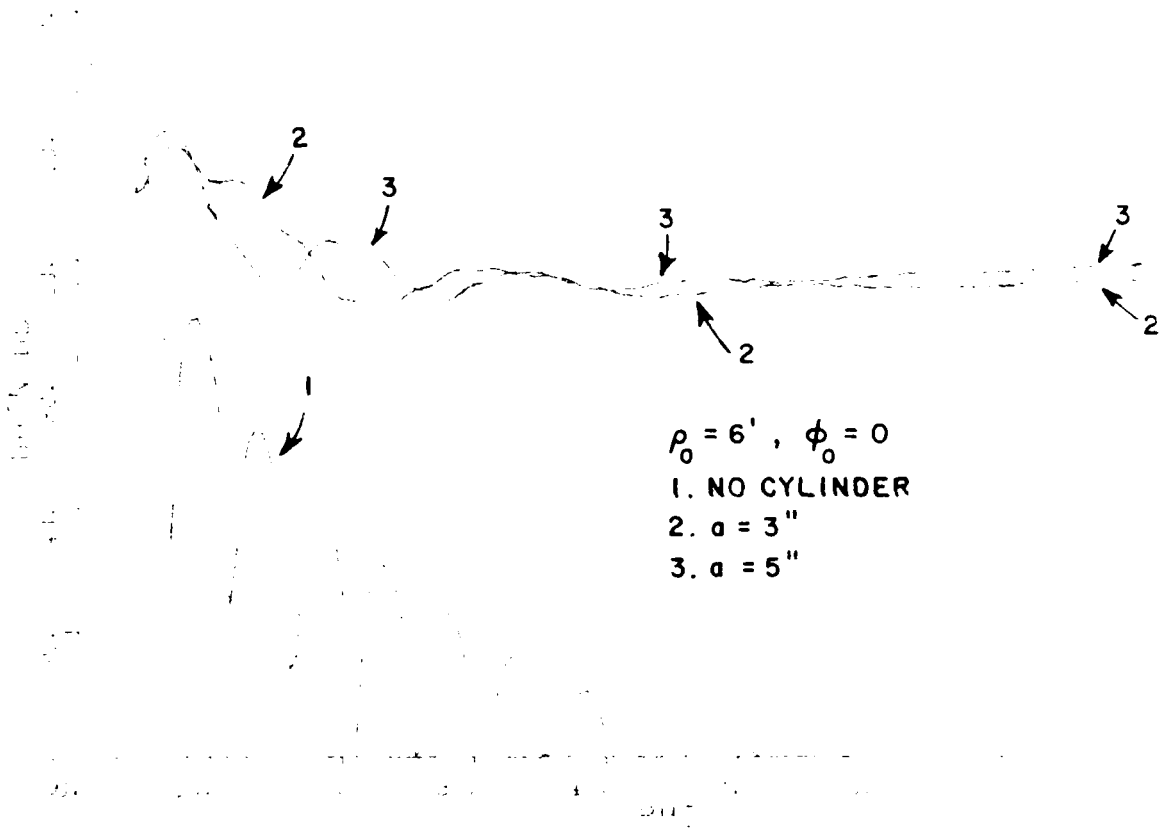

Figure 10. Azimuth pattern of the LAMPS antenna with a blocking cylinder. The on-axis blockage loss is 3.67 dB for a=3" and 6.43 dB for a=5".

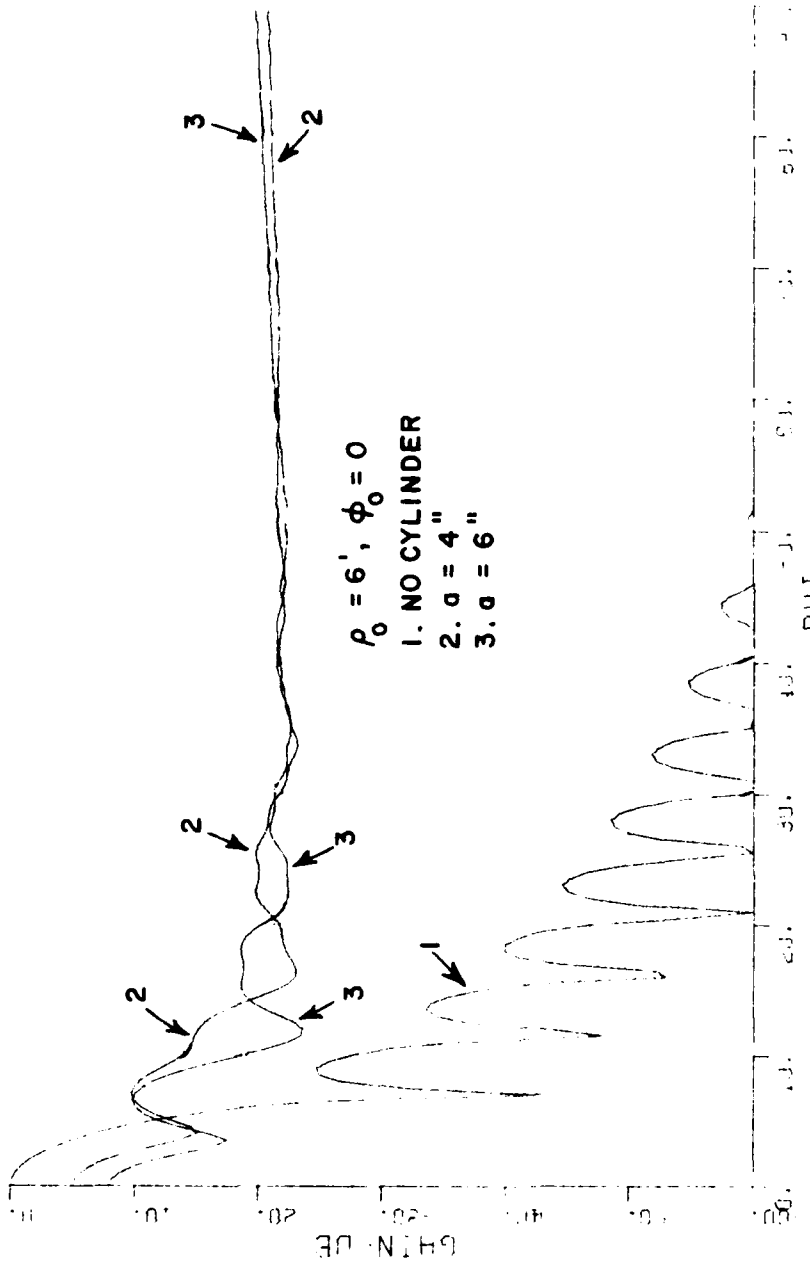

Figure 11. Azimuth pattern of the LAMPS antenna with a blocking cylinder. The on-axis blockage loss is 5.01 dB for a=4" and 7.96 dB for a=6".

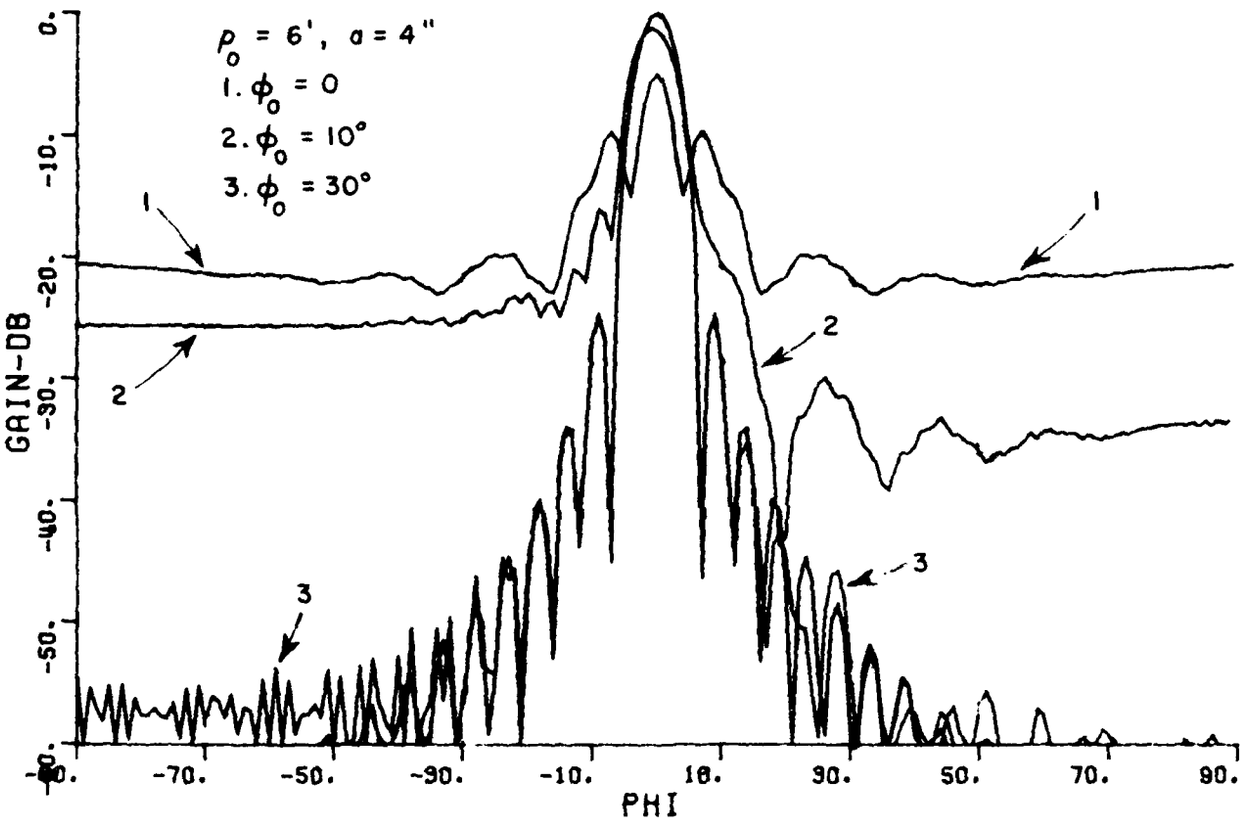

Figure 12. Azimuth pattern of the LAMPS antenna with a blocking cylinder.

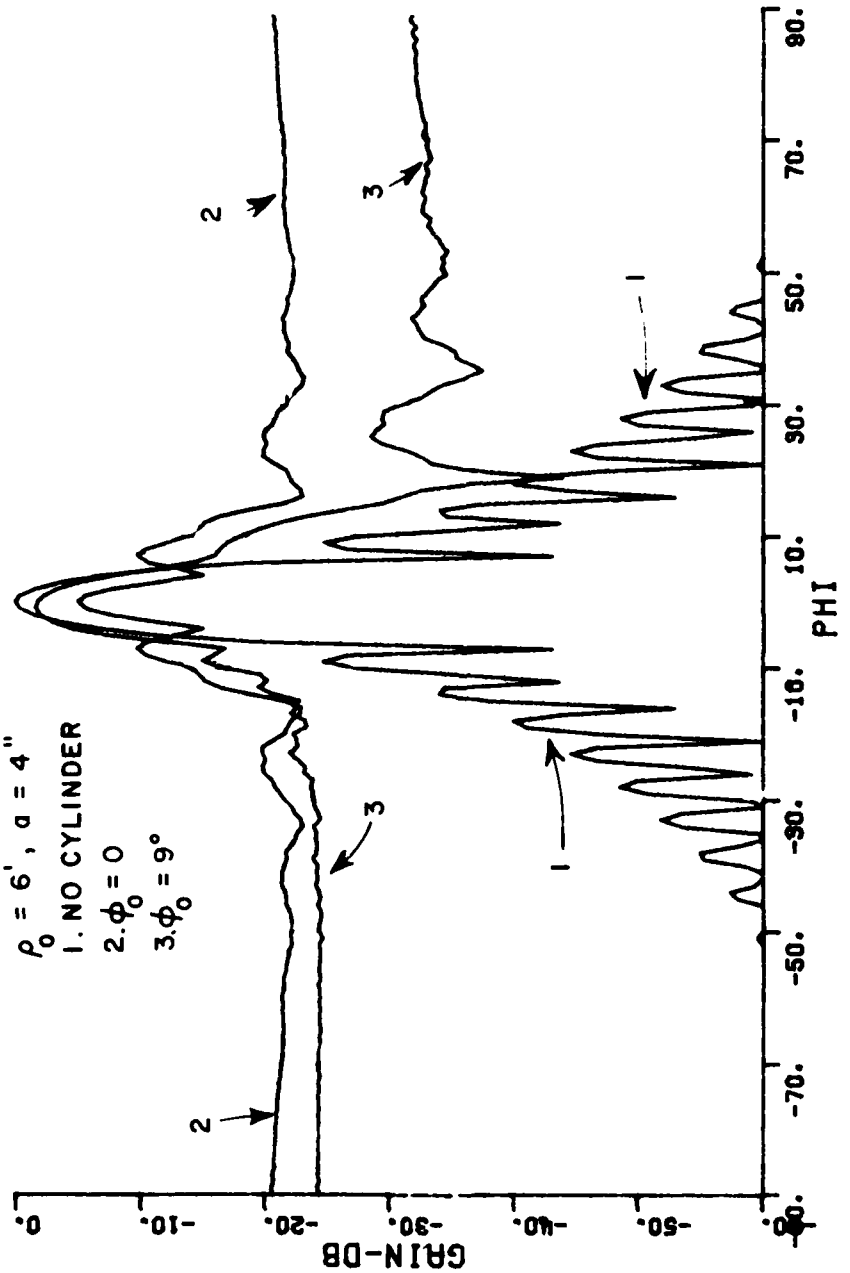

Figure 13. Azimuth pattern of the LAMPS antenna with a blocking cylinder.

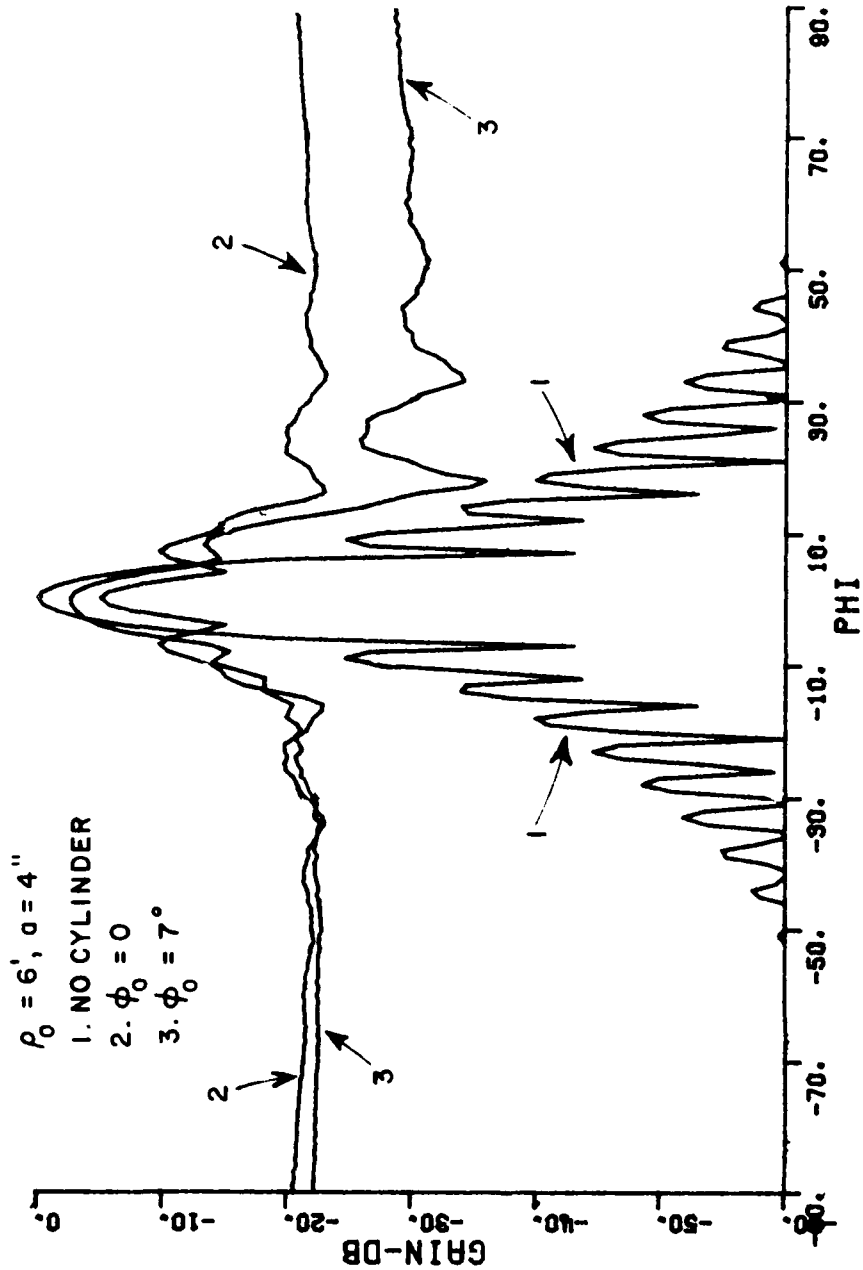

Figure 14. Azimuth pattern of the LAMPS antenna with a blocking cylinder.

V. CONCLUSIONS

An expression for the cylindrical diffraction coefficient suitable for use with circular cylinders has been developed. The diffraction coefficient is in the GTD format, and can be incorporated into a general, ray-optical analysis of a radiating system. Using this diffraction coefficient a computer code has been written which is capable of calculating antenna patterns for an aperture antenna in the vicinity of a circular conducting cylinder. At present the cylinder must be parallel to the plane of the aperture, and the pattern cut must be in the plane perpendicular to the cylinder axis. However, the theory needed for an extension of the code to the more general case is included herein. Recently these diffraction coefficients have been used to calculate the aperture blockage in the case of a reflector antenna with cylindrical feed supports [7].

Using this computer code the blockage effects of a 3" to 6" radius mast located 2 to 10 feet from the 34" diameter LAMPS antenna were calculated at 4.6 GHz. It was found that on-axis blockage, with the cylinder directly in front of the antenna ranged from -3.67 dB for a 3" radius cylinder to -7.96 dB for a 6" radius cylinder with the distance held constant at 6'. The on-axis blockage was affected very little by changing the antenna mast separation ρ_0, staying with $\pm$0.2 dB of -4.8 dB as ρ_0 varied from 2' to 10', with a 4" cylinder again located directly in front of the antenna. This insensitivity to mast-antenna separation is due to the fact that the mast is located well within the near field region of the LAMPS antenna for separations less than 30-40 feet. The on-axis blockage was found to decrease in the appropriate manner as ρ_0 was increased from 37.5 to 75 feet.

With ρ_0 held at 6 feet the on-axis blockage was reduced significantly as the mast was rotated from in front of the antenna. As ϕ_0 changed from 0° to 10° to 30° the on-axis blockage was reduced from -5.01 dB to -1.416 dB to 0.0 dB. In general, the amount of angular displacement of the mast away from on axis ($\phi_0 = 0°$) required to reduce the blockage below a given level is reduced by increasing ρ_0 the antenna-mast separation.

REFERENCES

[1] Kouyoumjian, R. G., and Pathak, P. H., "A Uniform Geometrical Theory of Diffraction for an Edge in a Perfectly Conducting Surface," Proceedings IEEE, Vol. 62, No. 11, November 1974.

[2] Kouyoumjian, R. G., "The Geometrical Theory of Diffraction and Its Application," Chapter 6 in Numerical and Asymptotic Techniques in Electromagnetics, Topics in Applied Physics, Vol. 3, edited by R. Mittra, Springer-Verlag, Berlin, 1975.

[3] Carter, P. S., "Antenna Arrays Around Cylinders," Proceedings IRE, Vol. 31, No. 12, December 1943.

[4] Wait, J. R., Electromagnetic Radiation from Cylindrical Structures, Pergamon Press, Chapter 4, 1959.

[5] Lucke, Winston S., "Electric Dipoles in the Presence of Elliptic and Circular Cylinders," Journal of Applied Physics, Vol. 22, No. 1, January 1951.

[6] Silver, S., Microwave Antenna Theory and Design, McGraw-Hill, 1949, p. 195.

[7] Lee, S. H., Rudduck, R. C., Klein, C. A., and Kouyoumjian, R. G., "A GTD Analysis of the Circular Reflector Antenna Including Feed and Strut Scatter," Final Technical Report 4381-1, May 1977, The Ohio State University Department of Electrical Engineering; prepared under Contract F30602-76-C-0224 for Department of the Air Force, Rome Air Development Center.

APPENDIX

THE FIELDS OF AXIAL DIPOLES IN THE PRESENCE OF A CIRCULAR CYLINDER

The geometry and coordinates are shown in Figure 1. The Green's function method will be used to find the radiated fields. Due to the nature of the problem, we need only find E_z, the z component of the electric field, for the electric dipole case, and H_z for the magnetic dipole case. As in the text, the cylinder is perfectly conducting. Once these components are found then

$$E_\theta = -E_z/\sin\theta \tag{A1}$$

$$E_\phi = \eta H_z/\sin\theta \tag{A2}$$

The scalar Green's functions of interest here satisfy the inhomogeneous partial differential equation

$$(\nabla^2 + k^2)\, G(\bar{r},\bar{r}') = -\delta(\bar{r}-\bar{r}') \tag{A3}$$

together with the radiation condition at infinity and certain boundary conditions on S. The Green's function $G_1(\bar{r},\bar{r}') = 0$ when $\bar{r}$ is on the cylindrical surface, whereas

$$\frac{\partial G_2}{\partial n'}(\bar{r},\bar{r}') = 0$$

when $\bar{r}$ is on the cylindrical surface. Here n' is taken in the direction normal to the cylindrical surface. For the circular cylinder

$$\frac{\partial}{\partial n'} = \frac{\partial}{\partial \rho} ,$$

$\bar{r}$ is the position vector for the field point (ρ,ϕ,z), and $\bar{r}'$ is the position vector for the source point (ρ',ϕ',z').

It can be shown that the solution to the boundary value problem for G_1 is

$$G_1(\bar{r},\bar{r}') = G_0(\bar{r},\bar{r}') + G_e(\bar{r},\bar{r}')$$

$$= \frac{-j}{8\pi} \sum_{m=0}^{\infty} \varepsilon_m \cos m(\phi-\phi') \int_{-\infty}^{\infty} \left[J_m'(\rho_<) - \frac{J_m(\rho_< a)}{H_m^{(2)}(\rho_< a)} H_m^{(2)\prime}(\rho_< a) \right] H_m^{(2)}(\rho_> a) H_m^{(2)}(\rho_< a) e^{jh(z-z')} dh$$

$$= \frac{1}{4\pi} \frac{e^{-jkR}}{R} + \frac{j}{8\pi} \sum_{m=0}^{\infty} \varepsilon_m \cos m(\phi-\phi') \int_{-\infty}^{\infty} \frac{J_m(\rho_< a)}{H_m^{(2)}(\rho_< a)} H_m^{(2)}(\rho_> a) H_m^{(2)}(\rho_< \rho') \times$$

$$\times e^{jh(z-z')} dh \qquad \text{(A4)}$$

in which

$G_0(R) = \frac{1}{4\pi} \frac{e^{-jkR}}{R}$ is the free-space Green's function,

$R = |\bar{r}-\bar{r}'|$ is the distance between the field and source points,

$\rho = \sqrt{k^2-h^2}$,

and the subscripts $<,>$ mean choose the value of ρ or ρ' whichever is smaller or larger, respectively.

In the far-zone one may replace $H_m^{(2)}(\rho_> \rho)$ by its large argument asymptotic approximation; furthermore $(z-z')$ is large, so the above integral in G_e may be evaluated asymptotically to obtain

$$G_e(\bar{r},\bar{r}') = \frac{-1}{4\pi} \frac{e^{-jkr}}{r} \sum_{m=0}^{\infty} \varepsilon_m j^m \frac{J_m(ka\sin\theta)}{H_m^{(2)}(ka\sin\theta)} \times$$

$$\times H_m^{(2)}(k\rho'\sin\theta)\cos m(\phi-\phi') \qquad \text{(A5)}$$

In this discussion the source is the electric current density

$$\bar{J}_v(\bar{r}') = p_e\, \delta(\bar{r}'-\bar{\rho}_o)\hat{z}\ , \tag{A6}$$

where the position vector $\bar{\rho}_o$ defines the source location (ρ_o,o,o) shown in Figure 1.

For such a z-directed source it follows from Maxwell's equations that

$$[\nabla^2 + k^2]E_z = j\omega\mu\left[1 + \frac{1}{k^2}\ \frac{\partial^2}{\partial z^2}\right]J_v\ . \tag{A7}$$

Using Green's second identity or comparing the above equation with (A3), it follows that

$$E_z(\bar{r}) = -j\omega\mu\left[1 + \frac{1}{k^2}\frac{\partial^2}{\partial z^2}\ \right]G_1(\bar{r},\bar{\rho}_o)p_e \tag{A8}$$

In the far-zone this simplifies to

$$E_z(r) = -jk\eta\, \sin^2\theta\ G_1(\bar{r},\bar{\rho}_o)p_e, \tag{A9}$$

where $\omega\mu$ has been replaced by $k\eta$. Thus from (A1), (A4), (A5) and (A9) and noting that

$$R \cong r - \rho_o\, \sin\theta\ \cos\phi$$

with $r >> \rho_o$ in the far-zone,

$$E_\theta = j\,\frac{k\eta}{4\pi}\,p_e\,\frac{e^{-jkr}}{r}\,\sin\theta\Big[e^{jk\rho_o\sin\theta\ \cos\phi} -$$

$$-\sum_{m=0}^{\infty}\varepsilon_m j^m\,\frac{J_m(ka\,\sin\theta)}{H_m^{(2)}(ka\,\sin\theta)}\,H_m^{(2)}(k\rho_o\sin\theta)\cos\,m\phi\Big], \tag{A10}$$

which is the same as (4) in the text.

The magnetic current moment (dipole) p_m gives rise to a z-directed electric field. The derivation of the expression for E_z closely parallels the proceding development. One starts with $G_2(\bar{r},\bar{r}')$ which has the same form as $G_1(\bar{r},\bar{r}')$ except that the ratio

$$\frac{J_m(ka)}{H_m^{(2)}(ka)} \text{ in } G_1 \text{ is replaced by } \frac{J_m'(ka)}{H_m^{(2)'}(ka)},$$

where the prime denotes differentiation with respect to the argument. Then following the steps taken in the preceding case and employing duality, we find that

$$H_z = -j \frac{k}{\eta} \sin^2\theta \; G_2(\bar{r},\bar{\rho}_o) p_m \tag{A11}$$

and so from (A2)

$$E_\phi = \frac{-jk}{4\pi} p_m \frac{e^{-jkr}}{r} \sin\theta \left[e^{jk\rho_o \sin\theta \cos\phi} - \right.$$

$$\left. - \sum_{m=0}^{\infty} \varepsilon_m j^m \frac{J_m'(ka \sin\theta)}{H_m^{(2)'}(ka \sin\theta)} H_m^{(2)}(k\rho_o \sin\theta) \cos m\phi \right], \tag{A12}$$

in the far-zone. The first term in the above equation is the field directly radiated from the magnetic dipole (the incident field), and the second term is the field diffracted by the cylinder. The second term is used to find the hard diffraction coefficient and so to define S_m in (22).

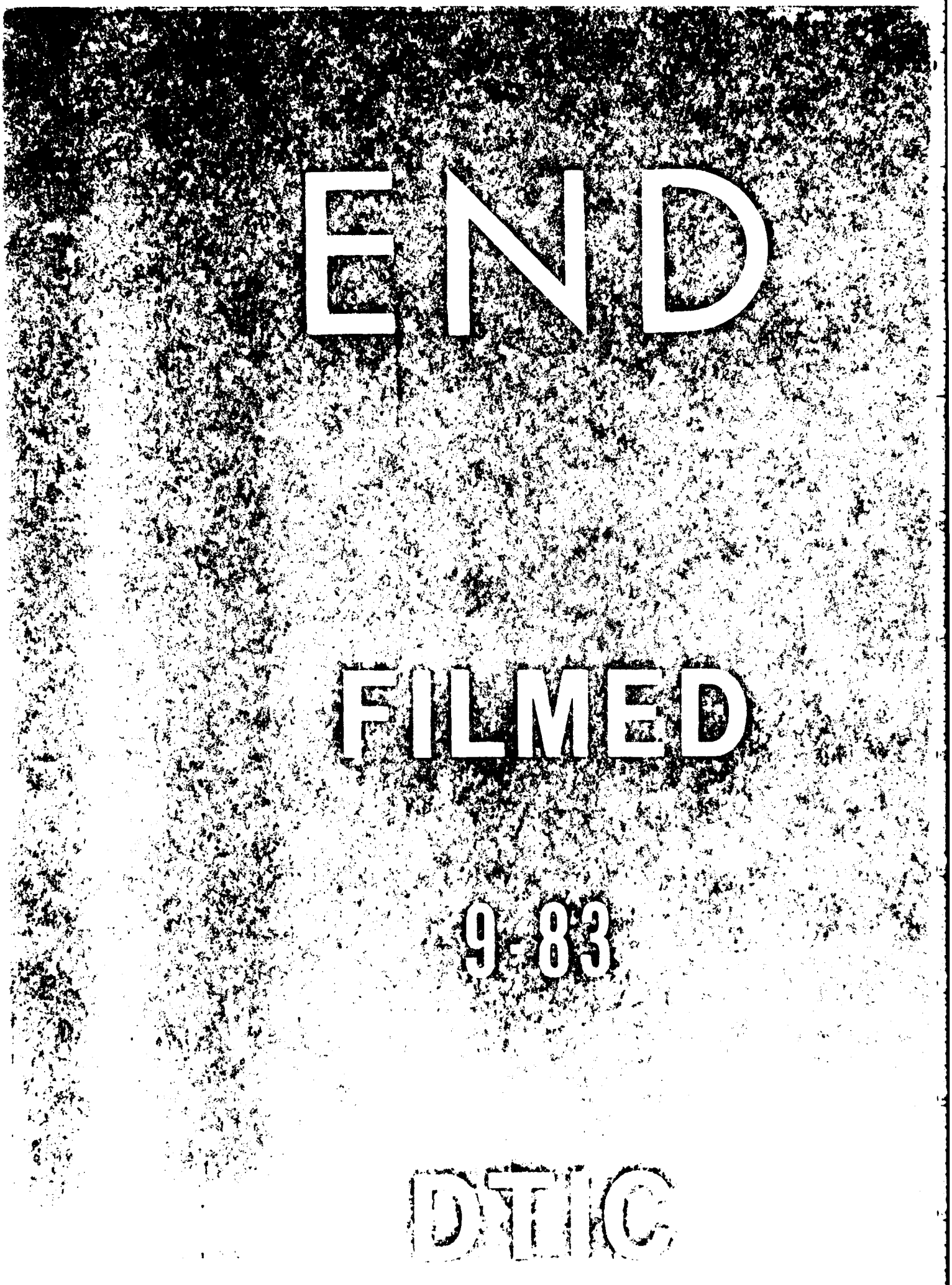
END
FILMED
9-83
DTIC